HHS Public Access

Author manuscript

J Comput Chem. Author manuscript; available in PMC 2018 April 05.

Published in final edited form as:

J Comput Chem. 2017 April 05; 38(9): 584–593. doi:10.1002/jcc.24715.

DelPhiForce, a tool for electrostatic force calculations: Applications to macromolecular binding

Lin Li[1], **Arghya Chakravorty**[1], and **Emil Alexov**[1,*]

[1]Department of Physics, Clemson University, Clemson, SC 29634, USA

Abstract

Long-range electrostatic forces play an important role in molecular biology, particularly in macromolecular interactions. However, calculating the electrostatic forces for irregularly shaped molecules immersed in water is a difficult task. Here we report a new tool, DelPhiForce, which is a tool in the DelPhi package that calculates and visualizes the electrostatic forces in biomolecular systems. In parallel, the DelPhi algorithm for modeling electrostatic potential at user-defined positions has been enhanced to include triquadratic and tricubic interpolation methods. The tricubic interpolation method has been tested against analytical solutions and it has been demonstrated that the corresponding errors are negligibly small at resolution 4 grids/Å. The DelPhiForce is further applied in the study of forces acting between partners of three protein-protein complexes. It has been demonstrated that electrostatic forces play a dual role by steering binding partners (so that the partners recognize their native interfaces) and exerting an electrostatic torque (if the mutual orientations of the partners are not native-like). The output of DelPhiForce is in a format that VMD can read and visualize, and provides additional options for analysis of protein-protein binding. DelPhiForce is available for download from the DelPhi webpage at http://compbio.clemson.edu/downloadDir/delphiforce.tar.gz.

Graphical abstract

A new tool, DelPhiForce, is developed and made available within DelPhi distribution to calculate and visualize electrostatic forces and torques acting between receptor and ligand. As illustrated in the figure, the electrostatic forces not only attract the binding partners to each other, but orient the ligand in the native binding mode via applying a torque that positions the native binding interfaces in the correct binding mode.

* ealexov@clemson.edu.

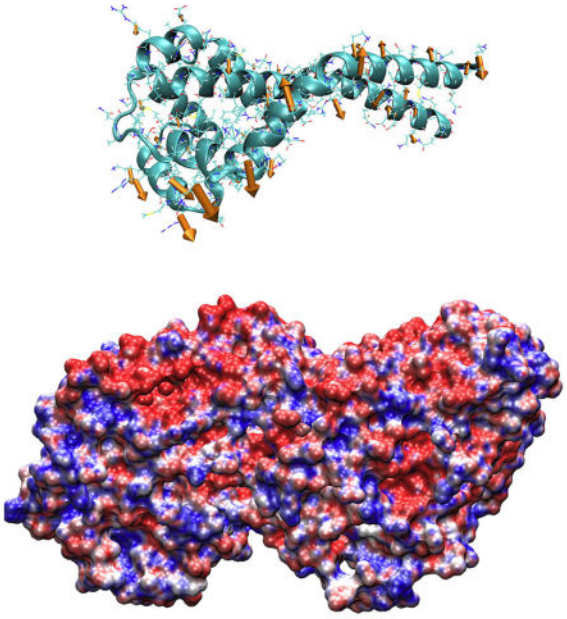

Keywords

macromolecular binding; Poisson-Boltzmann equation; electrostatic force; binding funnel; electrostatic interactions

Introduction

Electrostatic forces play an essential role in molecular biology and frequently dominate other effects [1,2]. It has been demonstrated that electrostatics provide a driving force for protein folding and stability [3–6], protein-protein binding [7–11], ion binding [12–14], dimerization [15,16], protein-DNA interactions [17,18], protein-microtubule binding [19], pKa values of ionizable groups [20,21], disease-causing SNPs [22–25] and many other biologically relevant phenomena [26]. Some aforementioned studies revealed the overall role of electrostatics, while others have focused on particular pair-wise interactions. These studies have predominantly focused on electrostatic potential and energy. However, it is equally important to model electrostatic forces and thus giving researchers the ability to predict plausible conformational changes and motions.

Pair-wise electrostatic interactions have been extensively utilized in the field of pKa calculations [20]. The pKa calculations methods relying on pair-wise interactions must compute the interaction energies between each pair of titratable groups and then apply a strategy to deliver the protonation states at a particular pH [27–34]. For this purpose, one needs computational tools to model the electrostatic interaction energy of the pairs (provided that all other charges are turned off). Various Poisson-Boltzmann (PB) solvers, such as DelPhi [35,36], PBSA [37,38], MIBPB [39] and APBS [40], offer such an option.

The field of molecular dynamics (MD) is another major direction in computational chemistry, requiring electrostatic forces to be computed at particular positions. Various

attempts have been made to model water phase in MD with a PB equation requiring the assignment of dielectric boundary/molecular surface forces to solute atoms [41–53]. Significant efforts were devoted to improve methods to facilitate the use of the PB models in MD simulations [54–62]. One of the earliest attempts was a variational approach to computing the total electrostatic force, with a special focus on numerical interpretation of the dielectric boundary forces [45] and the discontinuous dielectric constant model [48]. To enhance the numerical convergence and stability of dielectric boundary forces, a charge-based strategy was proposed [49,51]. Perhaps the most physically sound approach has been one in which the Maxwell stress tensor for the full nonlinear PBE system has been delivered, and can compute electrostatic forces with finite number of singularities while applying the discontinuous dielectric constant model [52].

Considering the PB approaches in which finite-difference technique to solve the PB equation is utilized, the electrostatic potential is delivered at the corresponding grid points. However, it is often the case that one might want to compute the potential (and force) at position(s) different from the grid points. Thus, the grid potential should be interpolated at user specified positions. Here we report a tricubic interpolation method implemented in DelPhi and a new force calculation tool, DelPhiForce, which computes electrostatic force between atoms, residues, or molecules. The DelPhiForce tool provides the forces of concerned systems and a file which can be visualized with VMD [63]. Using DelPhiForce, we demonstrate the role of electrostatics in the formation of protein-protein complexes. Three complexes are investigated: barnase-barstar [64], kinesin-tubulin [65], and dynein-tubulin [66]. It is demonstrated that electrostatic forces provide binding funnels leading the partners to the correct binding positions. Furthermore, electrostatic forces also provide an electrostatic torque that reorients the partners if their mutual orientation is not native-like.

Method

Calculating electrostatic potential, field and force

In the framework of continuum electrostatics, the electrostatic potential ϕ (in systems comprised of biological macromolecules and water in the presence of mobile ions) is calculated by solving the Poisson-Boltzmann equation (PBE), i.e.

$$\nabla \cdot [\varepsilon(\mathrm{r})\nabla\phi(\mathrm{r})] = -4\pi\rho(\mathrm{r}) + \varepsilon(\mathrm{r})\kappa^2(\mathrm{r})\sinh(\phi(\mathrm{r})/\mathrm{k_B T}) \quad (1)$$

where $\phi(\mathrm{r})$ is the electrostatic potential, $\varepsilon(\mathrm{r})$ is the dielectric permittivity, $\rho(\mathrm{r})$ is the permanent charge density, κ is the Debye-Huckel parameter, k_B is the Boltzmann constant and T is temperature. Due to the irregular shape of macromolecules, DelPhi uses finite difference (FD) method to solve the PBE.

Electrostatic field E(r) is the negative of the derivative of electrostatic potential $\phi(\mathrm{r})$. In the finite difference method, the electrostatic potential $\phi(\mathrm{r})$ is obtained at each grid(i, j, k) and is denoted as $\phi(\mathrm{i, j, k})$. Thus the E(i, j, k) components are calculated as:

$$\begin{cases} E_x(i,j,k) & = -[\phi(i,j,k) - \phi(i-1,j,k)]/h \\ E_y(i,j,k) & = -[\phi(i,j,k) - \phi(i,j-1,k)]/h \\ E_z(i,j,k) & = -[\phi(i,j,k) - \phi(i,j,k-1)]/h \end{cases} \quad (2)$$

where i, j, and k are the indices of finite difference grids in x, y, z directions, respectively, and h is the distance between two neighboring grids.

The FRC option in DelPhi

In many biologically relevant cases, the electrostatic potential, field, and force at a particular position(s) around a molecule can provide useful insights about macromolecular interactions. However, as mentioned above, electrostatic potential $\phi(r)$ is obtained on the grid points of the corresponding FD algorithm and these points may not reflect the desired position(s). Taking this into account, an option (the FRC option) is developed in DelPhi to obtain the electrostatic potential, field, and force at any arbitrary position(s). Here, three interpolation methods are implemented to interpolate the electrostatic potential, field, and force at any position(s).

Linear, quadratic and cubic interpolations

Three popular interpolation methods, namely trilinear, triquadratic, and tricubic interpolations, are explored and tested against the analytical examples (see the section entitled “the analytical examples” below). Among all three of these interpolation methods, trilinear interpolation is the most computationally efficient method. To obtain the electrostatic potential or field values at each desired position, only 8 (2^3) neighboring grids’ values are needed. Triquadratic and tricubic interpolation methods need 27 (3^3) and 64 (4^3) neighboring grids’ values, respectively. All three of the interpolation methods are implemented in DelPhi C++ version, which can be downloaded from: http://compbio.clemson.edu/delphi.

DelPhiForce work flow

The main purpose behind developing an algorithm for computing electrostatic forces, is to model electrostatic interactions. These interactions can be between proteins forming a complex, residues within the same protein, and atoms within the same molecule. Here we focus on protein-protein interactions simply to illustrate of one of the main applications of the method. Note that the FRC module of DelPhi is extensively used in the Multi Conformational Continuum Electrostatics (MCCE) method that predicts pKa values of protein ionizable groups [27,67]. Thus, consider a macromolecular complex comprised of receptor A and ligand B. If one wants to calculate the electrostatic potential, field, and force generated by the receptor A and acting on ligand B, the following procedure should be adopted (Fig 1): 1) The ligand B charges are turned off while the charges of the receptor A are kept as they are, 2) Provide atomic coordinates of ligand B atoms as an FRC input file (the electrostatic potential, field, and force will be calculated at these positions and output as an output FRC file), and 3) A file is generated in TCL format, which can be used to visualize

the forces in VMD [63]. The forces are represented by arrows in VMD. The size and direction of each arrow indicates the magnitude and direction of the corresponding force.

The analytical examples

To test FRC module and DelPhiForce module performance in conjunction with the aforementioned three interpolation methods, two analytical examples are created. The first example is a point charge in vacuum as shown in Fig 2a. The charge is set as +1 electron charge unit, while the size of the charge is set as 0.5 Å to mimic a point charge with no volume. A probe is used in the system, which has +1 electron charge unit and 0.5 Å radius. This probe is shifted from 4 Å to 10 Å away from the charge Q in steps of 0.1 Å. At each position, the electrostatic potential and force are calculated, both analytically and numerically by DelPhi. The shortest distance is set to be 4 Å, which is approximately the length of 2 radii of carbon or oxygen atoms.

The second example is a charge located in a spherical cavity in water. The spherical cavity is centered at origin (0,0,0) with a radius of R=12 Å. A charge of +10e is located 6 Å away from the origin (0,0,6). A probe charge, q=+1e, is used to test the electrostatic potential and forces around the cavity in the x–z plane, across 360 degrees in steps of 15 degrees. The distance between the probe and origin is d=15 Å. The cavity and charge system was created by ProNOI [68]. The analytical solution is described in supporting information.

To test the performance of different interpolation methods, the error and relative error of electrostatic potential is calculated for each test point. The error of potential is calculated as:

$$\varepsilon(\phi)=\phi_{\mathrm{num}}-\phi_{\mathrm{ana}} \quad (3)$$

where $\varepsilon(\phi)$ is the error of potential, ϕ_{num} is the numerical potential value, and ϕ_{ana} is the corresponding analytical potential value. A relative error (or normalized error) of potential is defined as:

$$\delta(\phi)=(\phi_{\mathrm{num}}-\phi_{\mathrm{ana}})/\phi_{\mathrm{ana}} \quad (4)$$

where $\delta(\phi)$ is the relative error of potential. Similar to equations (3) and (4), the error and relative error of electrostatic force are defined as:

$$\varepsilon(\mathrm{F})=\mathrm{F}_{\mathrm{num}}-\mathrm{F}_{\mathrm{ana}} \quad (5)$$

$$\delta(\mathrm{F})=(\mathrm{F}_{\mathrm{num}}-\mathrm{F}_{\mathrm{ana}})/\mathrm{F}_{\mathrm{ana}} \quad (6)$$

where $\varepsilon(F)$ is the error of force, F_{num} is the numerical force value, F_{ana} is the corresponding analytical force value, and $\delta(F)$ is the relative error of force. Note that in above equations (5,6), the magnitude of the force vector is taken.

The protein-protein complex examples

To demonstrate applications of the DelPhiForce, three protein-protein complexes are used as examples. The first complex is the Barnase-Barstar complex, PDB ID: 1BRS [64]. Chain A and chain D are used to model the barnase and barstar complex. The second case is the kinesin-tubulin complex structure with PDB ID: 4AQW [65]. The third structure is the dynein MTBD (microtubule binding domain)-tubulin complex structure, with PDB ID: 3J1U [66].

In order to calculate the binding forces between partners (referred to as A and B) within a complex as a function of distance and orientation, the following manipulations on the original structures are done. The monomer A is fixed in space, and monomer B is moved away from monomer A by 20 Å in the direction of the vector joining the mass centers of A and B. Then, monomer B is moved about the mass center vector in a circle with radius of 20 Å, which is on the plane perpendicular to the mass center vector. For each position of monomer B, the DelPhiForce is used to calculate the forces on residues of monomer B as well as the total force on monomer B.

In this work, we also investigate the rotation forces on binding monomers during the protein-protein association. For each complex structure, the monomer A is fixed in space, while the monomer B is moved away from monomer A by 20 Å, and the monomer B is rotated by 90 degrees. Then, the DelPhiForce is invoked to calculate the forces on residues of monomer B. To analyze the torsion forces, the monomer B is divided into two regions. For barstar and kinesin, the two regions are the interfacial residues and non-interfacial residues (where an “interfacial residue” is defined as a residue which has at least one atom in a <= 10 Å distance contact with the binding partner). For dynein structure, the two regions are the MTBD (microtubule binding domain) and the coiled coil stalk. The total force on each region is obtained and used to calculate the torsion force.

DelPhiPKa [34] is used to protonate the proteins at a pH value equal to 7. The force field used in the calculations for protein-protein complexes is charmm [69], the dielectric constants for water and protein are set as 80 and 2 respectively, the salt concentration is set at 0.15 mol/L, the resolution of the grid box (scale) is 4 grids per Å, and the surfaces of proteins are molecular surfaces [70] generated with a water probe radius of 1.4 Å.

DelPhi with the FRC option is written in C++. In order to be portable to all Linux and Mac systems, DelPhiForce is written in Bash script, which uses the DelPhi executable file. The output files of DelPhiForce are in text format and tcl script, which can be used for visualization purposes in VMD [63]. The DelPhiForce package is available online at http://compbio.clemson.edu/downloadDir/delphiforce.tar.gz. All the tests and calculations are done on Palmetto computer center (https://www.palmetto.clemson.edu/palmetto/).

Results and discussions

This section is organized as follows: the deficiency of the trilinear interpolation method for modeling electrostatic potential and force is demonstrated, then we show that higher order polynomial interpolations greatly reduce the error, and finally we illustrate the applicability of DelPhiForce on three receptor-ligand complexes.

Deficiency of trilinear interpolation

Trilinear interpolation method was already available in the previous version of DelPhi. Here we test it on analytical example 1. Thus, the electrostatic potential and force are benchmarked against the analytical values in three grid resolutions (or scales): scale=1, 2, and 4 grids/Å. Fig 3a and 3b show the potential and force comparisons among analytical methods and numerical methods applying different scales for DelPhiForce calculations. It can be seen that the calculated electrostatic potential is very close to the analytical values (Fig 3a). However, the calculated force deviates from the analytical one at close distances when using scale = 1.0 (Fig 3b).

To further analyze the errors in potential and force calculations, we show the errors (Fig 3(c,d)). The errors of potential and forces are calculated by subtracting corresponding analytical values from the numerical values. Fig 3c shows that the error of numerical solution decreases when the distance between the charge and the probe increases. The error clearly depends on the scale – a higher scale (or higher resolution) results in a smaller error. An interesting observation is that the error exhibits a periodical uphill and downhill performance. For example, when the scale=1, the period of the up and downhill pattern is 1 Å. The relatively low error points are at the distance equal to integer numbers. This effect occurs because all of the numerical values at the integer number distances are calculated by solving the Poisson-Boltzmann Equation (PBE). However, the values between each two integer distance points are determined by the trilinear interpolation method. Therefore, the uphill error is due to the trilinear interpolation method. Fig 3d shows the error of the forces, which exhibit very similar performance to the potential error in Fig 3c.

In further examination of the errors, we show the relative errors in Fig 3(e,f) (definitions of relative errors are provided in the method section, equations 3–6). The relative error exhibits similar periodical behavior as the absolute errors in Fig 3(c,d). At scale 2 grids/Å, which is the most commonly used resolution in DelPhi calculations, the relative error of electrostatic potential is less than 1 percent even at a distance of 4 Å. However, the relative error of force is about 3.5 percent at a distance of 4 Å, which is significantly larger than the relative error of potential. This is unsurprising as the force calculation is based on the electrostatic field calculation, which is calculated by taking the derivative of the electrostatic potential (see equation 2). Therefore, the upper bound of the relative error of force should be greater than the potential. Based on the analytical example test, the scale needs to be set at 4 grids/Å or higher in order to get less than 1 percent relative error of force calculation.

Higher-order polynomic interpolations

To reduce the error caused by the trilinear interpolation method, we implemented quadratic and cubic interpolations and compared the results against the analytical solution (Fig 4). The Fig 4 shows results obtained at scale =1 and 2 grids/Å only, because at scale=4 grids/Å the error and the relative error are too small to be visualized.

Fig 4 demonstrates that the trilinear interpolation method results in the largest error. Both triquadratic and tricubic interpolation methods improve the accuracy significantly. The lowest error is obtained by the tricubic interpolation method. When comparing triquadratic

and tricubic interpolation methods, several considerations should be made - in one dimensional case, the quadratic interpolation method takes three of the neighboring grids' values into account, while the cubic interpolation method takes four of the neighboring grids' values into account. Thus, in the case of quadratic interpolation, there are two options when choosing which three neighboring grids should be taken: left biased or right biased. The cubic interpolation does not have such a bias. Similarly, in the three-dimensional case, the triquadratic and tricubic interpolation methods take into account 27 (3^3) and 64 (4^3) neighboring grids' values, respectively. Thus, the tricubic interpolation has no bias in selecting neighboring grids. However, the tricubic interpolation needs more operations than the triquadratic interpolation. But such a difference in the operations can be ignored since either triquadratic or tricubic interpolation takes less than 0.1% in total computational time. Therefore, we consider that the tricubic interpolation is the best method for calculating the electrostatic potential and force.

Analytical example 2: a charge in cavity

To test the performance of the tricubic interpolation on a more realistic system with an analytical solution, we created the second analytical example, which is a charge in a spherical cavity and the charge is positioned offset from the geometrical center of the sphere. The sphere is assigned a low dielectric constant of 2, while the water phase has a dielectric constant of 80. The potential and force are calculated at points outside the sphere (15 Å away from the geometrical center along a circle with steps of 15 degrees. Details and the corresponding analytical solutions are provided in supporting information). In the DelPhiForce calculation, the scale is selected to be 4 grids/Å. The comparisons of potential and forces between DelPhi calculations and analytical solution are shown in Fig 5. The error of potential between DelPhi and analytical solution is in the range of 0.06 kT/e, and the error of force is less than 0.07 kT/(eÅ). This confirms the high accuracy achieved by implementing the tricubic interpolation.

Binding forces on protein complex examples

The DelPhiForce tool is developed to model the electrostatic forces between set of atoms, residues and molecules. Here we will illustrate its usage on several protein-protein complexes. Based on the analytical results, the default scale in DelPhiForce is 4 grids/Å; and the default interpolation method is tricubic.

The first case is the barnase-barstar complex (PDB ID: 1BRS) [64] (Fig 6a–d). The barnase-barstar complex has been examined in many research studies and is considered to be a classic testing example of a protein-protein docking problem [71–73]. The net charges of barnase and barstar are +2e and −6e, respectively. Furthermore, the charge distributions on both barnase and barstar are very inhomogeneous - the binding interface of barnase is strongly positively charged while the binding interface of barstar is quite negatively charged. The corresponding electrostatic forces are illustrated in Fig 6(a–d). Fig 6a shows the electrostatic potential of barnase mapped onto its molecular surface. One can clearly see the highly positively charged binding pocket (blue color in Fig 6). The barstar is moved away from its native binding position and purposely shifted around barnase (for clarity, Figs 6a and 6c show only two of these shifted positions, where barstar is in cartoon representation).

At each barstar position, the total electrostatic force exerted on barstar is calculated and illustrated as an arrow. The tail of an arrow is the mass center of the barstar and the length of an arrow is proportional to the magnitude of the electrostatic force. Figs 6b and 6d provide the same information, but barstar is removed for better visualization.

Another case is the kinesin's motor domain-tubulin complex (PDB ID 4AQW [65]), which is shown in Fig 6(e–h). Kinesin is a molecular motor that transports cargo along microtubules [74]. The net charges on kinesin and tubulin are +3e and −15e, respectively. The binding interface of kinesin is positively charged and the interface of tubulin is negatively charged. When the kinesin is positioned around the binding pocket of tubulin, the electrostatic forces attract the kinesin to the tubulin binding pocket. In Fig 6(e–h), surface representation of the tubulin is shown and electrostatic potential is mapped onto it. The kinesin is shown in cartoon representation. The arrows are the electrostatic forces generated by tubulin exerted on kinesin. Fig 6e and Fig 6f are the side views of the electrostatic forces with and without kinesin present, respectively. Fig 6g and Fig 6h are the top views of the electrostatic forces with and without kinesin present, respectively.

The third case is the dynein's MTBD (microtubule biding domain)-tubulin complex (PDB ID 3J1U). Dynein is also a molecular motor which transports cargo along microtubules [75]. Our previous work has demonstrated that the electrostatic interaction between dynein and tubulin helps dynein's microtubule binding domain (MTBD) dock into the binding pocket of tubulin [19]. In this work, we illustrate the electrostatic forces generated by tubulin and applied to dynein (Fig 6e–h). The net charges on tubulin and MTBD are −15e and 0e, respectively. The binding interface of tubulin is strongly negative, while the interface of MTBD is positive. In Fig 6(i–l), the tubulin is shown in surface representation with the electrostatic potential mapped onto it and the dynein MTBD is shown in cartoon representation. The arrows represent the electrostatic forces generated by tubulin and exerted on MTBDs. Fig 6i and Fig 6j are the side views of the electrostatic forces with and without dyneins present, respectively. Fig 6g and Fig 6h are the top views of the electrostatic forces with and without dyneins present, respectively.

All of the three examples demonstrate that electrostatic binding forces commonly exist in protein-protein complex systems. One can see that electrostatics provides guidance and drag the binding partner to the native binding position, even if the partner is not positioned correctly.

Torque in binding

Using these three protein-protein complexes, we investigate how electrostatic forces contribute to adjust the orientations of the ligand during the association processes. For each complex, we keep the receptor fixed and then move the ligand 20 Å away from the binding position, while rotating it by 90 degrees as shown in Fig 7 (see details in method section). Such a scenario models the case in which the binding partner is close to the binding pocket but the orientation is non-native. Fig 7(a,c,e) shows the electrostatic force on each residue while Fig 7(b,d,f) shows the corresponding torque.

These three cases demonstrate a common feature: the electrostatic forces not only guide the ligand towards the receptor, but also adjust its orientation so that the ligand binds to the receptor facing the native binding interface.

Conclusion

In this work, we reported newly developed features of DelPhi and an associated resource (DelPhiForce). Three interpolation methods were tested in the FRC option of DelPhi, including trilinear, triquadratic and tricubic interpolation methods. Based on our tests against analytical examples, the tricubic interpolation method was selected as the best method for the potential and force calculations. Furthermore, based on the results of the FRC option tests, we developed a DelPhiForce tool to calculate the electrostatic forces between set of atoms, residues, or molecules. DelPhiForce outputs the results in a text file and a script file is also provided for visualizing the forces with VMD.

The usage of DelPhiForce was demonstrated on three protein-protein complexes and it was shown that the new tool is successful in making two observations: 1.) the electrostatic forces guide the partners toward each other and provide steering towards the binding interfaces, and 2.) if the binding partners are not correctly oriented in relation to each other, the electrostatic forces result in a torque that re-orients the partners so that they approach each other in native binding mode orientation.

Supplementary Material

Refer to Web version on PubMed Central for supplementary material.

Acknowledgments

The work was supported by a grant from the Institute of General Medical Sciences, National Institutes of Health, award number R01GM093937.

References

1. Honig B, Nicholls A. Science. 1995; 268(5214):1144–1149. [PubMed: 7761829]
2. McCammon JA. Proceedings of the National Academy of Sciences of the United States of America. 2009; 106(19):7683–7684. [PubMed: 19416830]
3. Tsai MY, Zheng W, Balamurugan D, Schafer NP, Kim BL, Cheung MS, Wolynes PG. Protein science : a publication of the Protein Society. 2016; 25(1):255–269. [PubMed: 26183799]
4. Im W, Chen J, Brooks CL 3rd. Advances in protein chemistry. 2005; 72:173–198. [PubMed: 16581377]
5. Guest WC, Cashman NR, Plotkin SS. Biochemistry and cell biology = Biochimie et biologie cellulaire. 2010; 88(2):371–381. [PubMed: 20453937]
6. Strickler SS, Gribenko AV, Gribenko AV, Keiffer TR, Tomlinson J, Reihle T, Loladze VV, Makhatadze GI. Biochemistry. 2006; 45(9):2761–2766. [PubMed: 16503630]
7. Chakavorty A, Li L, Alexov E. Journal of computational chemistry. 2016; 37(28):2495–2507. [PubMed: 27546093]
8. Li L, Wang L, Alexov E. Frontiers in molecular biosciences. 2015; 2:5. [PubMed: 25988173]
9. Zhang Z, Witham S, Alexov E. Physical biology. 2011; 8(3):035001. [PubMed: 21572182]
10. Talley K, Ng C, Shoppell M, Kundrotas P, Alexov E. PMC biophysics. 2008; 1(1):2. [PubMed: 19351424]

11. Li L, Li C, Alexov E. Journal of Theoretical and Computational Chemistry. 2014; 13(03):1440002.
12. Petukh M, Alexov E. Asian journal of physics : an international quarterly research journal. 2014; 23(5):735–744. [PubMed: 25774076]
13. Petukh M, Zhenirovskyy M, Li C, Li L, Wang L, Alexov E. Biophysical journal. 2012; 102(12): 2885–2893. [PubMed: 22735539]
14. Petukh M, Zhang M, Alexov E. Journal of computational chemistry. 2015; 36(32):2381–2393. [PubMed: 26484964]
15. Campbell B, Petukh M, Alexov E, Li C. Journal of theoretical & computational chemistry. 2014; 13(3)
16. Zhang Z, Zheng Y, Petukh M, Pegg A, Ikeguchi Y, Alexov E. PLoS computational biology. 2013; 9(2):e1002924. [PubMed: 23468611]
17. Yang Y, Kucukkal TG, Li J, Alexov E, Cao W. ACS chemical biology. 2016
18. Kucukkal TG, Alexov E. Computational and mathematical methods in medicine. 2015; 2015:746157. [PubMed: 26064184]
19. Li L, Alper J, Alexov E. Scientific reports. 2016; 6:31523. [PubMed: 27531742]
20. Alexov E, Mehler EL, Baker N, Baptista AM, Huang Y, Milletti F, Nielsen JE, Farrell D, Carstensen T, Olsson MH, Shen JK, Warwicker J, Williams S, Word JM. Proteins. 2011; 79(12): 3260–3275. [PubMed: 22002859]
21. Wang L, Li L, Alexov E. Proteins. 2015; 83(12):2186–2197. [PubMed: 26408449]
22. Petukh M, Li M, Alexov E. PLoS computational biology. 2015; 11(7):e1004276. [PubMed: 26146996]
23. Kucukkal TG, Petukh M, Li L, Alexov E. Current opinion in structural biology. 2015; 32:18–24. [PubMed: 25658850]
24. Stefl S, Nishi H, Petukh M, Panchenko AR, Alexov E. Journal of molecular biology. 2013; 425(21):3919–3936. [PubMed: 23871686]
25. Teng S, Madej T, Panchenko A, Alexov E. Biophysical journal. 2009; 96(6):2178–2188. [PubMed: 19289044]
26. Dias RP, Li L, Soares TA, Alexov E. Journal of computational chemistry. 2014; 35(19):1418–1429. [PubMed: 24799021]
27. Georgescu RE, Alexov EG, Gunner MR. Biophysical journal. 2002; 83(4):1731–1748. [PubMed: 12324397]
28. Alexov EG, Gunner MR. Biochemistry. 1999; 38(26):8253–8270. [PubMed: 10387071]
29. Alexov EG, Gunner MR. Biophysical journal. 1997; 72(5):2075–2093. [PubMed: 9129810]
30. Carstensen T, Farrell D, Huang Y, Baker NA, Nielsen JE. Proteins. 2011; 79(12):3287–3298. [PubMed: 21744393]
31. Meyer T, Knapp EW. Journal of chemical theory and computation. 2015; 11(6):2827–2840. [PubMed: 26575575]
32. Meyer T, Kieseritzky G, Knapp EW. Proteins. 2011; 79(12):3320–3332. [PubMed: 21744394]
33. Kieseritzky G, Knapp EW. Proteins. 2008; 71(3):1335–1348. [PubMed: 18058906]
34. Wang L, Li L, Alexov E. Proteins: Struct, Funct, Bioinf. 2015; 83(12):2186–2197.
35. Li L, Li C, Sarkar S, Zhang J, Witham S, Zhang Z, Wang L, Smith N, Petukh M, Alexov E. BMC biophysics. 2012; 5:9. [PubMed: 22583952]
36. Li C, Petukh M, Li L, Alexov E. Journal of computational chemistry. 2013; 34(22):1949–1960. [PubMed: 23733490]
37. Wang C, Wang J, Cai Q, Li Z, Zhao HK, Luo R. Computational & theoretical chemistry. 2013; 1024:34–44. [PubMed: 24443709]
38. Botello-Smith WM, Liu X, Cai Q, Li Z, Zhao H, Luo R. Chemical physics letters. 2013; 555:274–281. [PubMed: 23439886]
39. Zhou Y, Zhao S, Feig M, Wei GW. Journal of Computational Physics. 2006; 213(1):1–30.
40. Baker NA, Sept D, Joseph S, Holst MJ, McCammon JA. Proceedings of the National Academy of Sciences. 2001; 98(18):10037–10041.
41. Davis ME, McCammon JA. Journal of computational chemistry. 1990; 11(3):401–409.

42. Sharp K. Journal of computational chemistry. 1991; 12(4):454–468.
43. Zauhar RJ. Journal of computational chemistry. 1991; 12(5):575–583.
44. Niedermeier C, Schulten K. Molecular Simulation. 1992; 8(6):361–387.
45. Gilson MK, Davis ME, Luty BA, McCammon JA. Journal of Physical Chemistry. 1993; 97(14): 3591–3600.
46. Cortis CM, Friesner RA. Journal of computational chemistry. 1997; 18(13):1591–1608.
47. Im W, Beglov D, Roux B. Comput Phys Commun. 1998; 111(1–3):59–75.
48. Che J, Dzubiella J, Li B, McCammon JA. J Phys Chem B. 2008; 112(10):3058–3069. [PubMed: 18275182]
49. Cai Q, Ye X, Wang J, Luo R. Chemical physics letters. 2011; 514(4–6):368–373. [PubMed: 22125339]
50. Li B, Cheng X, Zhang Z. Siam Journal on Applied Mathematics. 2011; 71(6):2093–2111. [PubMed: 24058212]
51. Cai Q, Ye X, Luo R. Phys Chem Chem Phys. 2012; 14(45):15917–15925. [PubMed: 23093365]
52. Xiao L, Cai Q, Ye X, Wang J, Luo R. The Journal of Chemical Physics. 2013; 139(9):094106. [PubMed: 24028101]
53. Xiao L, Wang C, Luo R. Journal of Theoretical and Computational Chemistry. 2014; 13(03): 1430001.
54. Gilson MK. Journal of computational chemistry. 1995; 16(9):1081–1095.
55. Friedrichs M, Zhou RH, Edinger SR, Friesner RA. J Phys Chem B. 1999; 103(16):3057–3061.
56. Lu BZ, McCammon JA. Journal of chemical theory and computation. 2007; 3(3):1134–1142. [PubMed: 26627432]
57. Geng WH, Wei GW. Journal of Computational Physics. 2011; 230(2):435–457. [PubMed: 21088761]
58. Xiao L, Wang C, Ye X, Luo R. J Phys Chem B. 2016; 120(33):8707–8721. [PubMed: 27146097]
59. Juffer AH, Botta EFF, Vankeulen BAM, Vanderploeg A, Berendsen HJC. Journal of Computational Physics. 1991; 97(1):144–171.
60. Vorobjev YN, Grant JA, Scheraga HA. J Am Chem Soc. 1992; 114(9):3189–3196.
61. Yoon BJ, Lenhoff AM. Journal of Physical Chemistry. 1992; 96(7):3130–3134.
62. Luty BA, Davis ME, McCammon JA. Journal of computational chemistry. 1992; 13(6):768–771.
63. Humphrey W, Dalke A, Schulten K. Journal of molecular graphics. 1996; 14(1):33–38. [PubMed: 8744570]
64. Buckle AM, Schreiber G, Fersht AR. Biochemistry. 1994; 33(30):8878–8889. [PubMed: 8043575]
65. Goulet A, Behnke-Parks WM, Sindelar CV, Major J, Rosenfeld SS, Moores CA. Journal of Biological Chemistry. 2012; 287(53):44654–44666. [PubMed: 23135273]
66. Redwine WB, Hernández-López R, Zou S, Huang J, Reck-Peterson SL, Leschziner AE. Science. 2012; 337(6101):1532–1536. [PubMed: 22997337]
67. Gunner MR, Zhu X, Klein MC. Proteins. 2011; 79(12):3306–3319. [PubMed: 21910138]
68. Smith N, Campbell B, Li L, Li C, Alexov E. BMC structural biology. 2012; 12(1):31. [PubMed: 23217202]
69. Vanommeslaeghe K, Hatcher E, Acharya C, Kundu S, Zhong S, Shim J, Darian E, Guvench O, Lopes P, Vorobyov I. Journal of computational chemistry. 2010; 31(4):671–690. [PubMed: 19575467]
70. Rocchia W, Sridharan S, Nicholls A, Alexov E, Chiabrera A, Honig B. Journal of computational chemistry. 2002; 23(1):128–137. [PubMed: 11913378]
71. Sheinerman FB, Honig B. Journal of molecular biology. 2002; 318(1):161–177. [PubMed: 12054776]
72. Katchalski-Katzir E, Shariv I, Eisenstein M, Friesem AA, Aflalo C, Vakser IA. Proceedings of the National Academy of Sciences. 1992; 89(6):2195–2199.
73. Li L, Guo D, Huang Y, Liu S, Xiao Y. BMC bioinformatics. 2011; 12(1):1. [PubMed: 21199577]
74. Hirokawa N, Noda Y, Tanaka Y, Niwa S. Nature reviews Molecular cell biology. 2009; 10(10): 682–696. [PubMed: 19773780]

75. Miki H, Okada Y, Hirokawa N. Trends in cell biology. 2005; 15(9):467–476. [PubMed: 16084724]

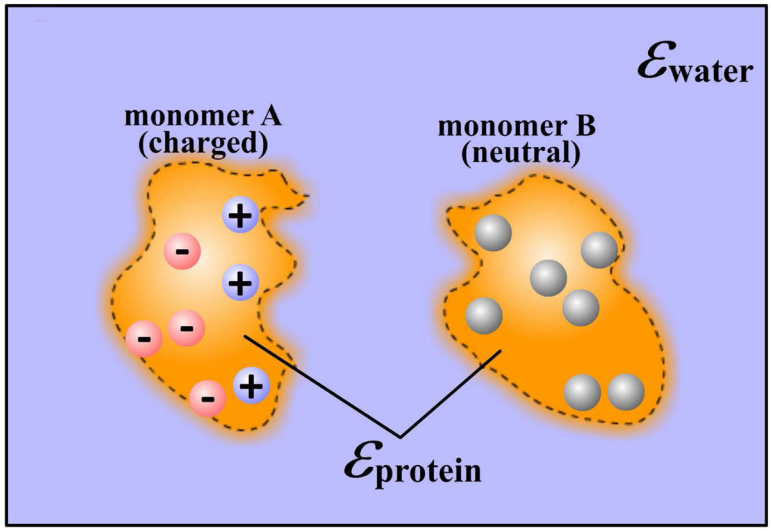

Fig. 1. Illustration of the usage of the DelPhiForce module protocol

The receptor charges are kept as specified by the corresponding force field parameters, while the ligand charges are turned off. Both the receptor and the ligand are immersed in a water phase with a high dielectric constant, while the interior of the macromolecules is treated with a low dielectric constant.

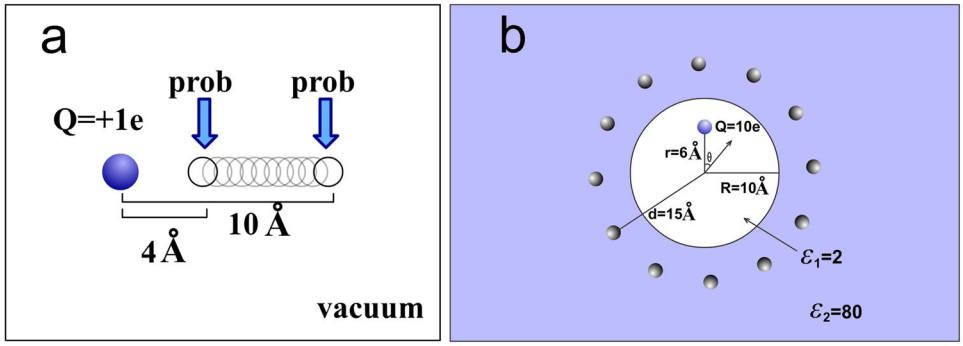

Fig. 2. Analytical examples for testing the performance of the FRC module

(a) charged atom in vacuum acting on a probe. (b) spherical cavity with single charge offset the center, generating potential and forces on probe positions shown as small grey spheres. The system is immersed in water.

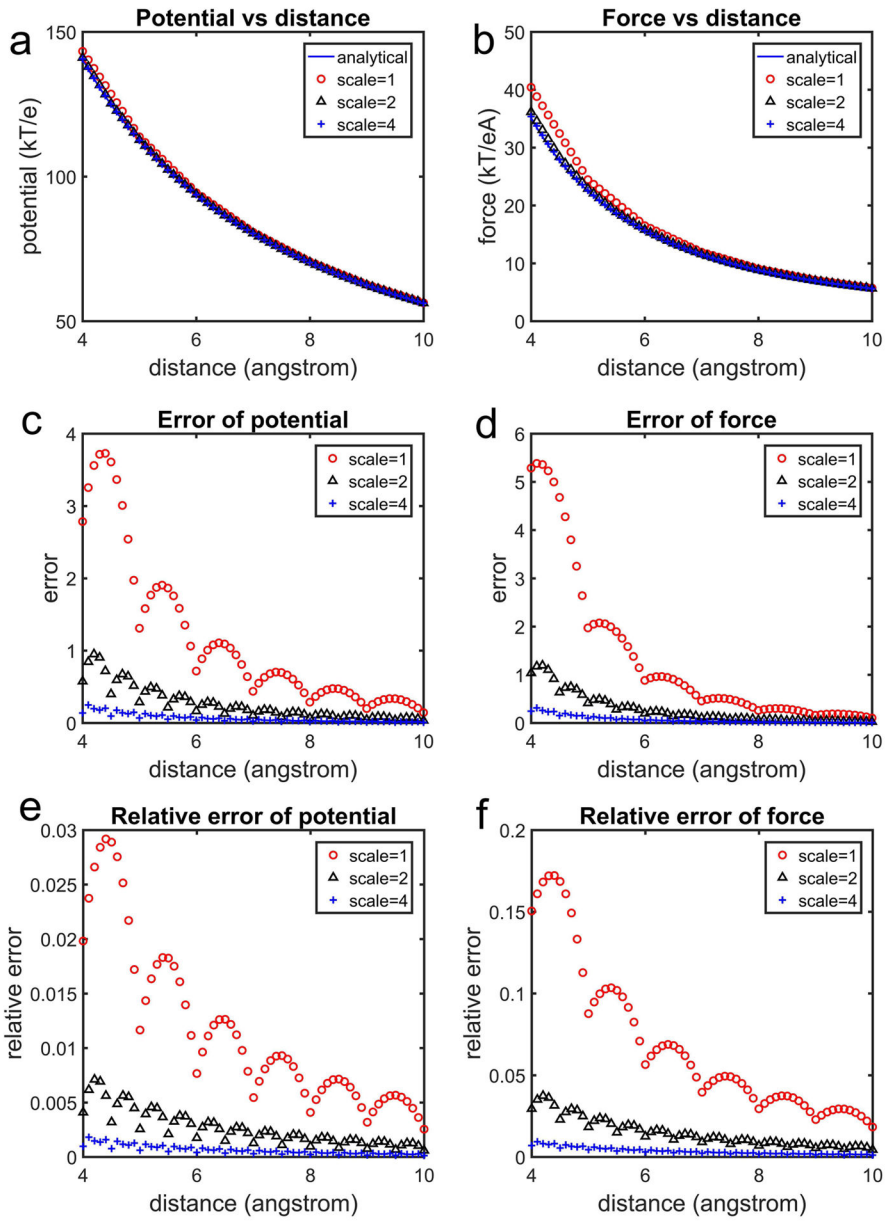

Fig. 3. The results (electrostatic potential and force) obtained using the trilinear interpolation method

Upper panels plot the potential and force as a function of distance, the middle panels the corresponding errors, and bottom panels the relative error. The value of scale is in grids per Angstrom.

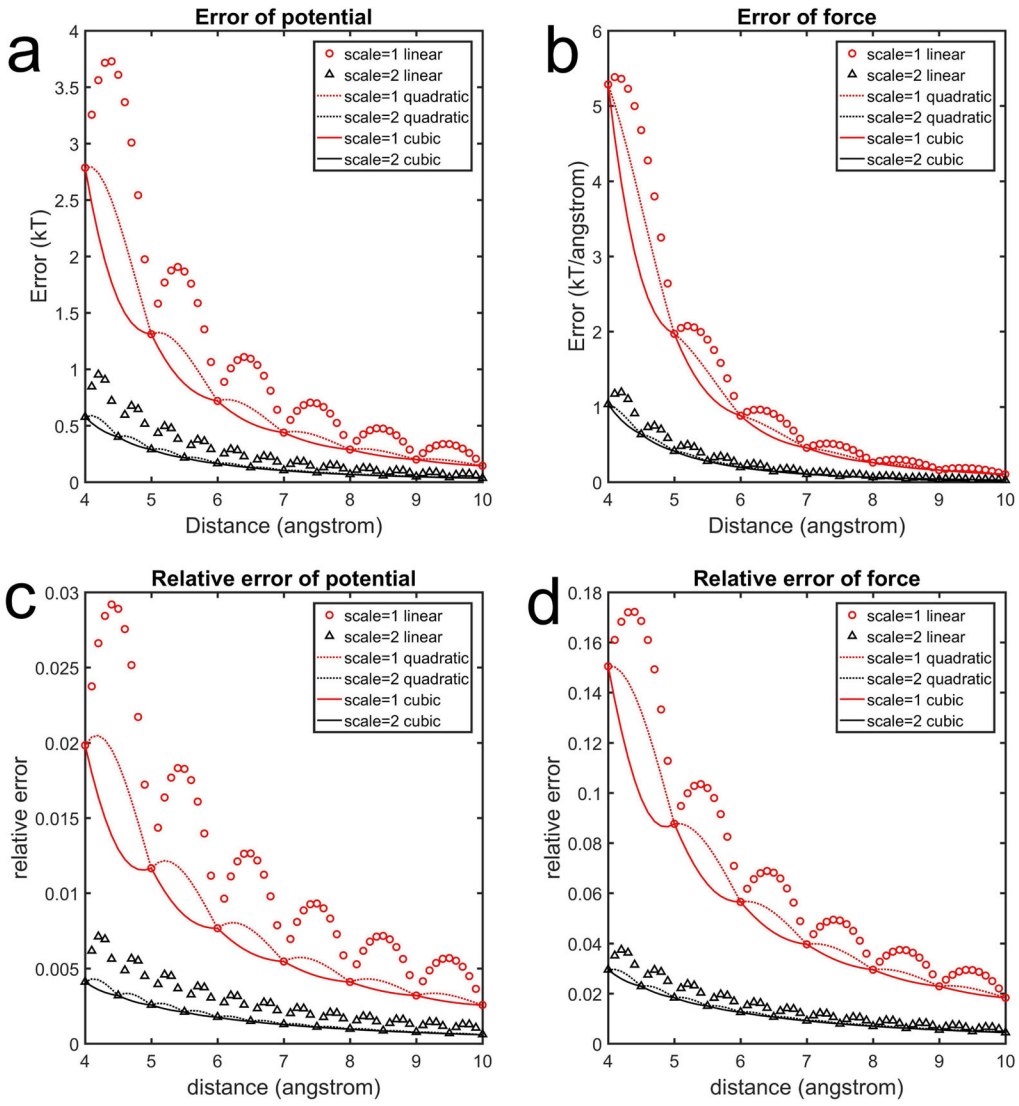

Fig. 4. The comparison between trilinear, triquadratic, and tricubic interpolations

The upper panel shows the error as a function of the distance (the potential on the left, and the force on the right). The bottom panel shows the relative error of the same quantities.

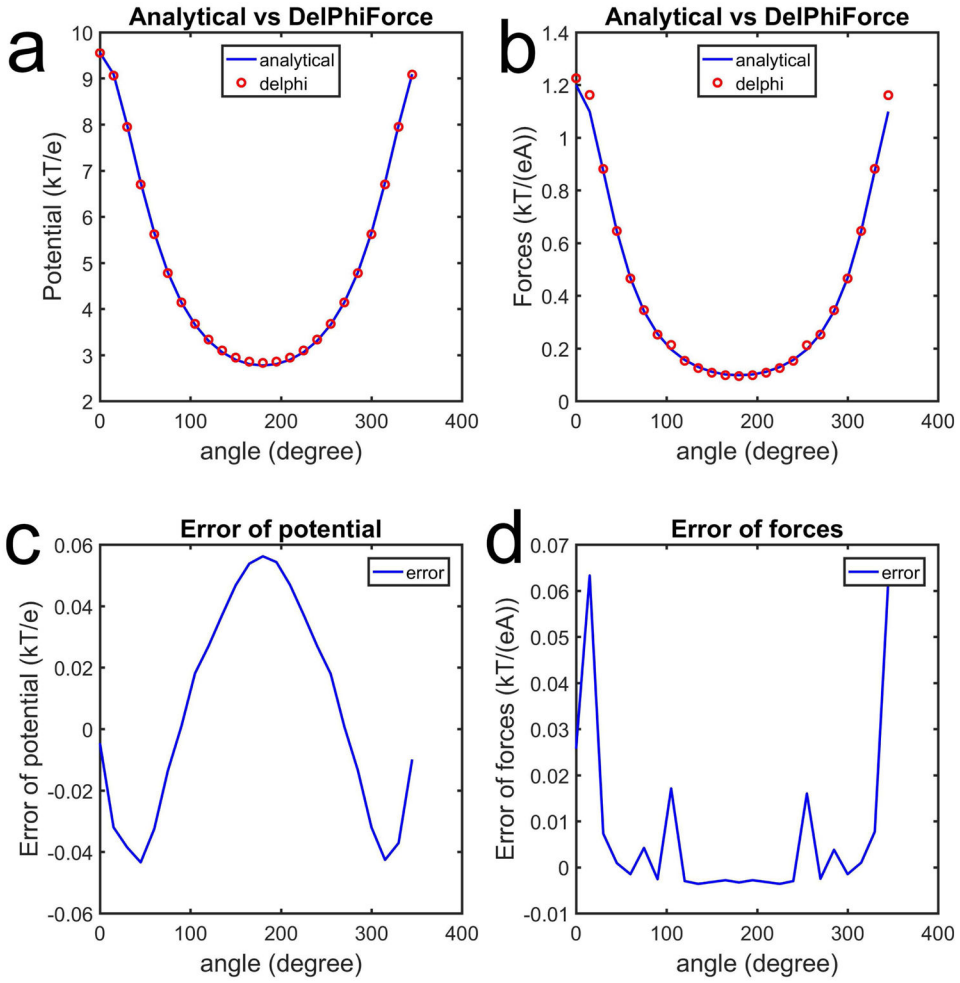

Fig. 5. The comparison between DelphiForce results and the analytical solution of analytical example 2

The upper panels show the potential and force as a function of the polar angle. The bottom panels show the corresponding errors.

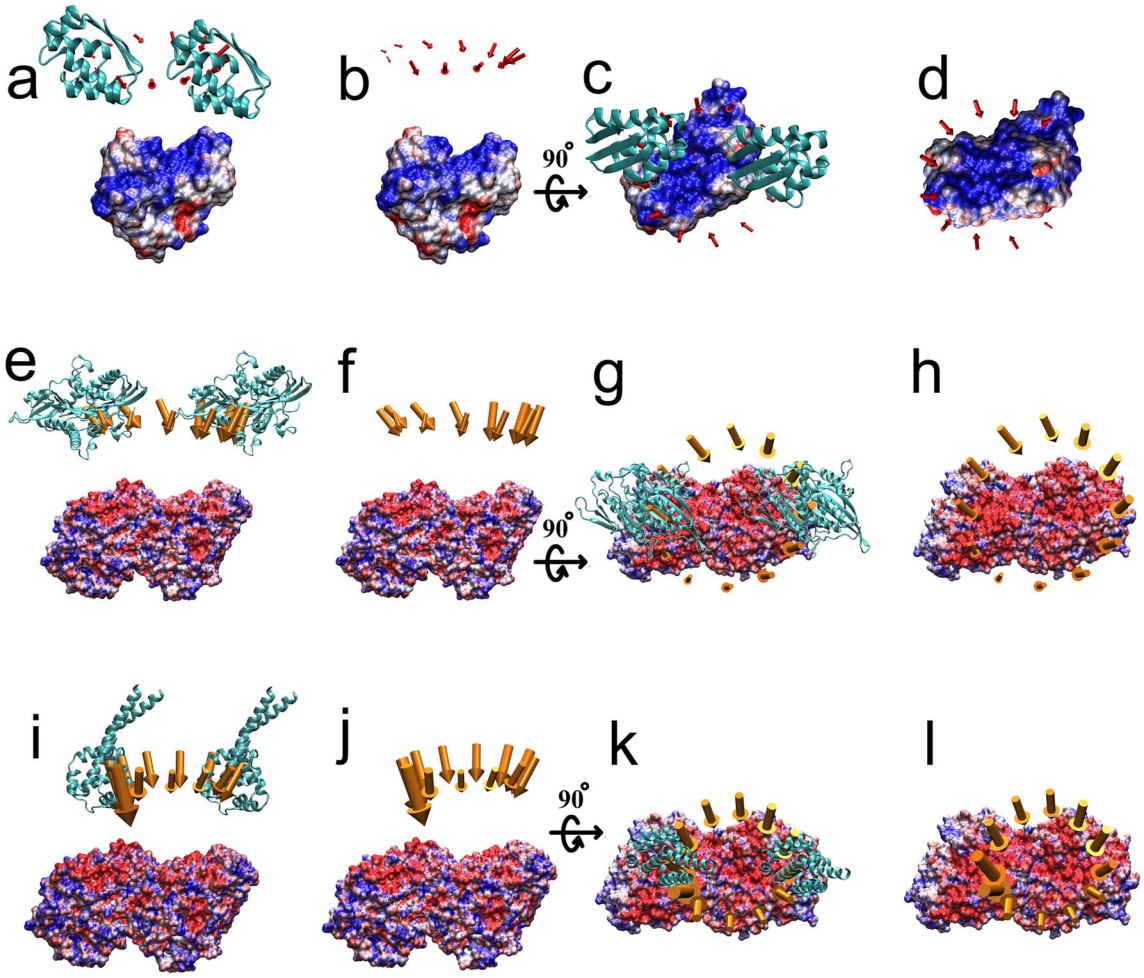

Fig. 6. Electrostatic forces calculated with DelPhiForce and visualized with VMD

The electrostatic forces are shown as arrows, with the tail of each arrow representing the mass center of the binding partner and the length of each arrow being proportional to the magnitude of the electrostatic force. In the first row, panels a–d show the barnase-barstar complex. In the middle row, panels e–h show the tubulin-kinesin complex. In the bottom row, panels i–l show the tubulin-dynein complex. The receptor (barnase, tubulin, tubulin) is shown in surface presentation with electrostatic potential mapped onto it. The ligand (barstar, kinesin, dynein) is shown in cartoon presentation.

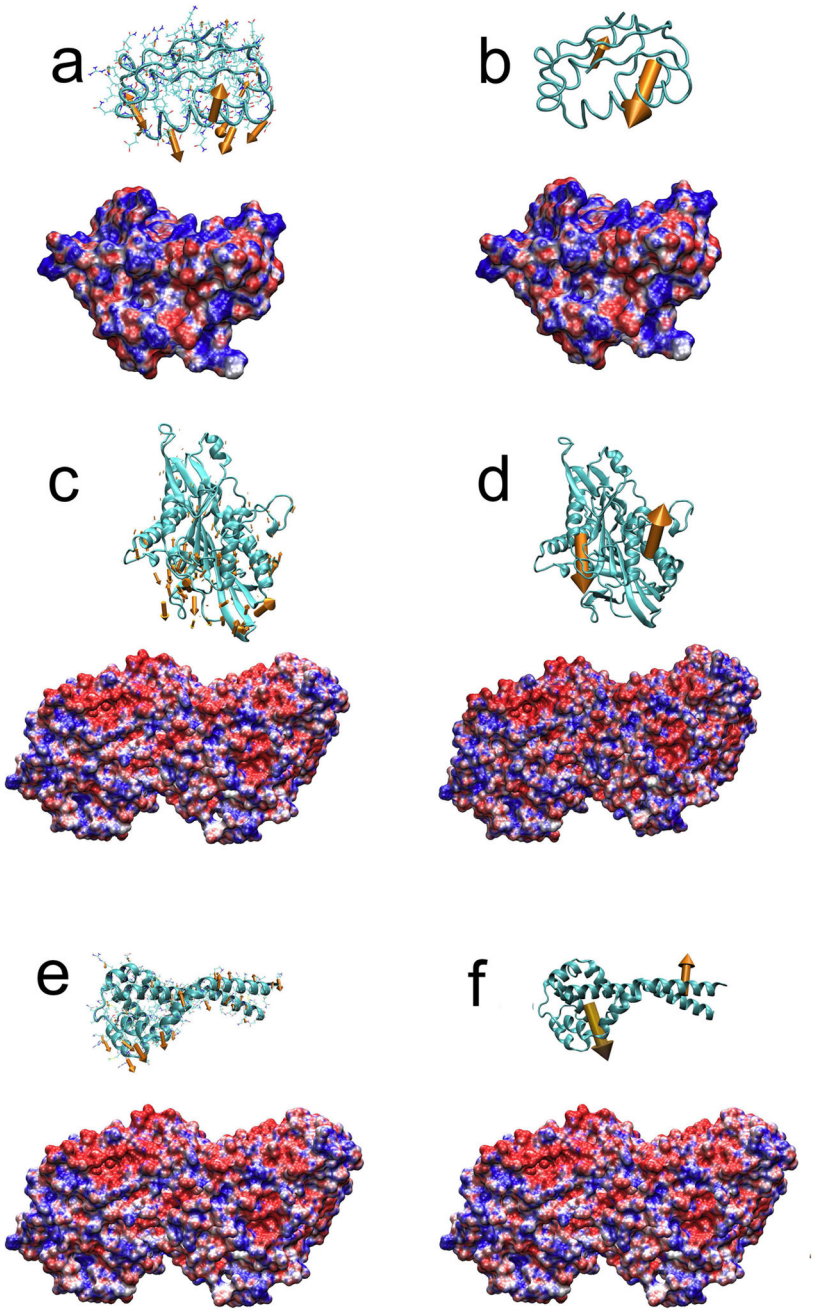

Fig. 7. The electrostatic forces and the corresponding torque acting on the ligand, in the case where the ligand is rotated 90 degrees away from its native orientation

In the first row, panels a–b show the barnase-barstar complex. In the middle row, panels c–d show the tubulin-kinesin complex. In the bottom row, panels e–f show the tubulin-dynein complexes. First column shows the electrostatic forces generated by the receptor on each residue of the ligand. Second column demonstrates the corresponding torque. The receptor is shown in molecular surface presentation with electrostatic potential mapped onto it. The ligand is shown in cartoon presentation.